Nonlinear control for stabilization of small neoclassical tearing modes in ITER

2012 Nucl. Fusion 52 063007

(http://iopscience.iop.org/0029-5515/52/6/063007)

IOP Publishing and International Atomic Energy Agency Nuclear Fusion
Nucl. Fusion **52** (2012) 063007 (14pp) doi:10.1088/0029-5515/52/6/063007

Nonlinear control for stabilization of small neoclassical tearing modes in ITER

B.A. Hennen[1,2], M. Lauret[1,2], G. Hommen[1,2], W.P.M.H. Heemels[2], M.R. de Baar[1,2] and E. Westerhof[1]

[1] FOM Institute for Plasma Physics 'Rijnhuizen', Association EURATOM-FOM, Trilateral Euregio Cluster, PO Box 1207, 3430 BE Nieuwegein, The Netherlands
[2] Eindhoven University of Technology, Control Systems Technology Group/Hybrid and Networked Systems Group, PO Box 513, 5600 MB Eindhoven, The Netherlands

E-mail: b.a.hennen@tue.nl

Received 23 September 2011, accepted for publication 27 March 2012
Published 17 April 2012
Online at stacks.iop.org/NF/52/063007

Abstract
In this paper, the feasibility of feedback stabilization of neoclassical tearing modes at small island sizes, corresponding to otherwise unstable island sizes in ITER scenario 2, is demonstrated. The islands are stabilized by application of electron cyclotron resonance heating and current drive in a regime where the application of current drive in open loop normally results in a complete suppression of the island. By applying current drive in closed loop with feedback of real-time measurements of the island width, complete suppression is avoided and the island is stabilized at a specific reduced size. In contrast to complete suppression, control of islands at a specific size will allow the manipulation of a plasma's current density profile in hybrid scenarios. Three conceptual (non-)linear feedback controllers with varying complexity, performance, robustness and required model knowledge are introduced. Simulations show the theoretical feasibility of small island stabilization at a specific reduced width. The controllers are applied to the generalized Rutherford equation, which governs the island evolution subject to electron cyclotron current drive. A strategy for the gradual implementation of the controllers is suggested. Stabilization of small islands by feedback control will allow the use of system identification to extend the model knowledge on the evolution of small islands, and in addition will extend the operational regime.

(Some figures may appear in colour only in the online journal)

1. Introduction

Suppression of magnetic islands [1] is a requirement for the operation of ITER [2]. This is particularly relevant for the high β-scenarios with sawteeth, in which neoclassical tearing modes (NTMs) are likely to be destabilized. NTMs are initiated by seed islands [1] that are created in the magnetic field by other magnetohydrodynamic (MHD) events [3]. The seed reduces the pressure gradient over the island, as a consequence of which the local bootstrap current is reduced. After seeding of the NTM, the island grows to a saturated size $w = w_{\mathrm{sat}}$. The width of a magnetic island w is usually reduced by applying localized electron cyclotron resonance heating and current drive (ECRH/ECCD) on the island. As a consequence of this reduction of the island size the NTM is suppressed.

Full suppression of NTMs has been demonstrated on several tokamaks, see [1, 4] and references therein. However, one could also consider stabilization of the NTM at a specific island size. A peculiarity of NTMs, subject to ECRH/ECCD, is the existence of unstable equilibrium island widths below a certain threshold island size, referred to as w_{thres}. Usually, a large fraction of the available ECRH/ECCD power is applied in open loop to bring the island size below w_{thres}, after which the island vanishes by itself [1, 5, 6], i.e. applying a sufficiently large level of ECRH/ECCD power results in $\mathrm{d}w/\mathrm{d}t < 0$ for all w and consequently $w \to 0$. NTM suppression requires precise alignment of ECRH/ECCD with the island centre. Several methods for radial alignment of the ECRH/ECCD deposition and the mode rational surface r_{s} were experimentally demonstrated in a closed feedback loop [7–10]. In [10], experimental results are described, which demonstrate autonomous alignment of the suppressing ECRH/ECCD power deposition with a 2/1 tearing mode using a dedicated real-time control system. This system is based on a steerable ECRH/ECCD launcher and a line-of-sight ECE diagnostic [11]. The applied ECRH/ECCD power P_{ec} in these experiments is modulated, to deposit power in the island's centre or O-point only.

An important aspect of the open-loop application of ECRH/ECCD for the suppression of an island is that often the maximum available power $P_{\mathrm{ec,\ max}}$ is applied, or that an *a priori* model-prediction of the required power P_{ec} is used

to ensure a complete suppression [1]. Instead of complete suppression one could also consider stabilization of NTMs at specific sizes. It was recently presented [12, 13] that islands in high-performance discharges influence the ambient plasma, e.g. islands are observed to cause flux pumping, which can positively affect the evolution of the current density profile. The results shown in [12, 13] suggest that direct control over the island width thus allows for actuation of the ambient plasma.

This paper analyses stabilization of small NTMs using feedback techniques. For an effective stabilization of the mode, a feedback loop can be conceived in which the applied ECRH/ECCD power is manipulated in response to real-time measurements of the island width w. This implies the real-time computation of the controlled variable P_{ec} as a function of the real-time measured $w(t)$: $P_{ec}(w(t))$. In this numerical study, it will be shown that using the feedback law $u(w) = P_{ec}(w)$, NTMs can be stabilized at small sizes below the threshold width $w < w_{thres}$. Three feedback controllers will be introduced and simulated to demonstrate this in theory. An experimental verification of the approaches discussed here is outside the scope of this paper but will be carried out in the near future. The analysis presented here will be restricted to the control of $m/n = 2/1$ NTMs below w_{thres} in ITER scenario 2 discharges [14].

The average power required to keep the island at a constant size below w_{thres} will hold important information on the small island physics. For small islands, a finite pressure gradient remains over the island, and hence the bootstrap current is not completely suppressed. This implies that the precise ratio between the parallel and perpendicular heat diffusivity becomes important [1, 15, 16]. Secondly, the exact effect of the ion polarization current is not well known [1, 15, 16]. As the discussion on these small island physics is still ongoing and outside the scope of this paper, we will use a simplified model which gives a generic description of the evolution of NTM dynamics only. It will be shown that such a simplified model is sufficient to design controllers for the NTM stabilization problem.

Section 2 of this paper introduces the generalized Rutherford equation (GRE), following [17, 18]. The GRE describes the dynamics of the NTM. In section 3, the relevant parameter set for ITER scenario 2 is listed [14]. In section 4, the equilibria of the GRE for different operating points at constant P_{ec} are calculated and the dynamics of the GRE are analysed. In sections 5, 6 and 7, controllers with varying complexity, performance and robustness are introduced. A gradual implementation of these controllers is proposed, starting with a standard linear proportional integral (PI) controller. This controller is derived and applied in simulation to show the stabilization of islands at small island sizes $w < w_{thres}$. It will be shown that the control performance obtained with this controller can only be guaranteed locally in close vicinity of the chosen operating point, i.e. near a certain island size. In order to optimize the control performance in a broader, global domain, two nonlinear controllers are proposed thereafter. A sliding mode controller [19, 20] is introduced and simulated, followed by a controller based on feedback linearization [20]. Both nonlinear controllers explicitly compensate the nonlinear island dynamics, resulting in an optimal control performance in a broad operational domain. The merits of the three different control methods will be outlined both theoretically and in simulation. A comparison of the three control strategies is given in section 8. Section 9 assesses issues related to the practical implementation of the control methods for stabilization of NTMs in ITER. Implications for implementation of the NTM stabilization techniques in experiments are discussed. The effect of parameter uncertainties on the performance of the designed controllers is briefly discussed. In addition to parametrical uncertainties, the designed controllers should also deal with uncertainties on the functional dependence of the bootstrap current representation in the GRE at small island sizes. Such uncertainties are not considered further in the analysis presented here as it is expected that the derived controllers can be made robust for such uncertainties in a practical setup. Section 10 employs one of the controllers for pre-emptive closed-loop stabilization of an NTM at a small size. Section 11 summarizes the results and draws the conclusions.

2. Generalized Rutherford equation

The evolution of the NTM island width w, i.e. its growth dynamics, are governed by the GRE [1, 21]. The expressions for the different stabilizing and destabilizing terms differ from the expressions used for classical tearing modes. In the rest of this work, it is assumed that the applied ECRH/ECCD is perfectly aligned with the island centre. Note that it is probable that the alignment in ITER will not be very accurate [22]. However, for the problem of stabilizing an island at a specific width in a feedback loop that manipulates the applied ECRH/ECCD power, the effect of a less accurate alignment will have no consequences for the stability of the system. Here, the GRE is used in its generalized form as presented in [17, 18]:

$$0.82\frac{\tau_r}{r_s}\frac{dw}{dt} = r_s\Delta'_0 + r_s\Delta'_{BS} + r_s\Delta'_{CD}. \quad (1)$$

r_s is the radius of the mode's rational surface, Δ'_0 is the classical tearing index, Δ'_{BS} a term accounting for the lacking bootstrap current related drive of the island and Δ'_{CD} a term representative of ECCD. Note that in this case, only the current drive effect of the applied ECRH/ECCD is implicitly taken into account in the model, as the suppression of NTMs in ITER is dominated by the direct non-inductive current drive effect of the applied EC waves [17, 23]. Note furthermore that the rotation of the NTMs is not included in this model. The different terms of the GRE are averaged over one rotation period of the island. A resistive diffusion time scale τ_r is introduced, which is defined as

$$\tau_r = \frac{\mu_0\kappa r_s^2}{\eta_{neo}}, \quad (2)$$

where the neoclassical resistivity is given by

$$\eta_{neo} = 2.8\times10^{-8}Z_{eff}T_{sep}^{-3/2}(1-\varepsilon^{1/2})^{-2}, \quad (3)$$

with μ_0 the magnetic permeability, Z_{eff} the effective charge, T_{sep} the average electron temperature at the island separatrix and $\varepsilon = r_s/R_0$ the inverse aspect ratio. R_0 is the major radius and κ is a parametrization representing the plasma elongation.

Consider the case with $r_s\Delta'_{CD} = 0$, i.e. without applying ECRH/ECCD to the island. Realize that without application of

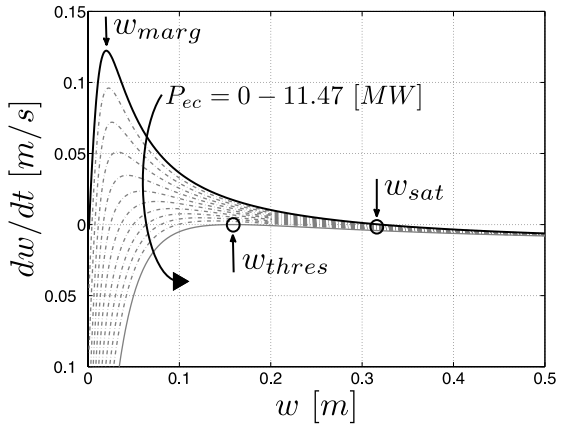

Figure 1. Solution of the GRE plotting $\mathrm{d}w/\mathrm{d}t$ versus w for different values of applied ECRH/ECCD power P_{ec}. Up to 11.47 MW of ECRH/ECCD is applied to the $m/n = 2/1$ NTM to suppress the mode from its saturated width $w_{\mathrm{sat}} = 0.32$ m to a certain suppressed width. The solid black curve is the solution for the case where no ECRH/ECCD is applied ($P_{\mathrm{ec}} = 0$) and the mode grows to its saturated width w_{sat} where $\mathrm{d}w_{\mathrm{sat}}/\mathrm{d}t = 0$. The results depicted are obtained by combining the GRE (1) with the transport model of equation (5).

ECRH/ECCD, the mode saturates at the stable saturated island width w_{sat}, with $\mathrm{d}w_{\mathrm{sat}}/\mathrm{d}t = 0$, see figure 1. Consequently, for a saturated NTM, the following static relation between Δ'_0 and Δ'_{BS} must hold:

$$\Delta'_0 = -\Delta'_{\mathrm{BS}}(w \equiv w_{\mathrm{sat}}). \tag{4}$$

For NTMs in ITER, Δ'_0 is typically stabilizing, i.e. negative $\Delta'_0 < 0$. The destabilizing contribution to the growth of the mode is usually considered to originate from a few distinct physics mechanisms. The destabilization of NTMs is mainly attributed to a perturbed helical bootstrap current, which reinforces the growth of an initial seed island. The term Δ'_{BS} relates to the perturbed bootstrap current. At small island sizes, however, the perturbed bootstrap current is not sufficient to initiate the seeding and growth of NTMs. The perturbed bootstrap current term in the expression is therefore modified by a term related to the finite parallel transport near an NTM island, which results in an incomplete flattening of the pressure gradient inside the magnetic island, modifying the GRE. Combining the bootstrap current term and the transport term yields

$$r_{\mathrm{s}}\Delta'_{\mathrm{BS}} = \frac{16\mu_0 L_q r_{\mathrm{s}}}{B_{\mathrm{pol}}\pi}\frac{4}{3w}\frac{w^2}{\left(w^2 + w^2_{\mathrm{marg}}\right)} j_{\mathrm{BS}}, \tag{5}$$

where μ_0 is the vacuum magnetic permeability, r_{s} the radial mode location, $L_q \equiv q/(\mathrm{d}q/\mathrm{d}r)$ the local magnetic shear length at r_{s}, B_{pol} the local poloidal magnetic field component at r_{s}, and j_{BS} the bootstrap current. The marginal island width w_{marg} is defined as the island width for which the growth rate $\mathrm{d}w/\mathrm{d}t$ is maximum, see figure 1.

An alternative expression, for the term Δ'_{BS}, is related to the combination of the perturbed helical bootstrap current with the so-called ion polarization effect. In this case, for small island sizes, the limitation of the neoclassical drive of the island width is attributed to a stabilizing ion polarization effect, where the assumption should be satisfied that the marginal island size is expected to scale with the ion banana width. The alternative expression for $r_{\mathrm{s}}\Delta'_{\mathrm{BS}}$ reads

$$r_{\mathrm{s}}\Delta'_{\mathrm{BS}} = \frac{16\mu_0 L_q r_{\mathrm{s}}}{B_{\mathrm{pol}}\pi}\frac{4}{3w}\left(1 - \frac{w^2_{\mathrm{marg}}}{3w^2}\right) j_{\mathrm{BS}}. \tag{6}$$

Both expressions are also used in [6]. As stated in the introduction, the detailed contribution of these two mechanisms is not known. In the GRE used here, only expression (5) will be taken into account. Since this work focuses on the development of methodologies for feedback stabilization of otherwise unstable magnetic island sizes, a detailed model based on physics interpretation is not required. The model should just give a sufficient description of the qualitative, global dynamics of the NTM suppression process. Particularly, the polarization term will be neglected here. It is expected that the actual behaviour of Δ'_{BS} at small island sizes can be identified in experiments during the gradual introduction of the controllers.

By insertion of relation (5) in equation (4) the following static relation is obtained:

$$r_{\mathrm{s}}\Delta'_0 = -\frac{16\mu_0 L_q r_{\mathrm{s}}}{B_{\mathrm{pol}}\pi}\frac{4}{3w_{\mathrm{sat}}}\frac{w^2_{\mathrm{sat}}}{\left(w^2_{\mathrm{sat}} + w^2_{\mathrm{marg}}\right)} j_{\mathrm{BS}}. \tag{7}$$

Next, the contribution of the stabilizing ECRH/ECCD is added to the expression of the GRE following [17, 18]:

$$r_{\mathrm{s}}\Delta'_{\mathrm{CD}} = -\frac{16\mu_0 L_q}{B_{\mathrm{pol}}\pi}\frac{\eta_{\mathrm{cd}} P_{\mathrm{ec}}}{w^2_{\mathrm{dep}}} N_{\mathrm{CD}}\left(w/w_{\mathrm{dep}}\right), \tag{8}$$

with

$$N_{\mathrm{CD}}\left(w/w_{\mathrm{dep}}\right) = \frac{0.25 + 0.24(w/w_{\mathrm{dep}})}{1 + 0.64(w/w_{\mathrm{dep}})^3 + 0.43(w/w_{\mathrm{dep}})^2 + 1.5(w/w_{\mathrm{dep}})}, \tag{9}$$

and $P_{\mathrm{ec}}(t)$ is the applied heating or current drive power, w_{dep} is the full width of the power deposition and η_{CD} is the global current drive efficiency. N_{CD} is a normalized, analytical function describing the geometrical distribution of the EC power. Note that in [17, 18], Δ'_{CD} is explicitly expressed as a function of the alignment accuracy of ECRH/ECCD with the mode rational surface r_{s}. Since we assume a perfect alignment, the expression of Δ'_{CD} is simplified here by leaving the dependence on the alignment accuracy out of consideration. Note furthermore that throughout this paper P_{ec} is considered as a constant power input. The effect of power modulation is not incorporated in the model and its influence on the small island physics is neglected here. This assumption is justified since modulation switches at a much faster time scale than the island width evolution in ITER. If one would like to take the effect of modulation into account, the models should not only be extended with a modulation part but also would have to incorporate a rotation model, which would make the model less suitable for a controller design study.

3. ITER parameter set

Table 1 gives an overview of the parameters of the ITER scenario 2, which is used for further analysis and simulation

Table 1. Parameters GRE.

$P_{\mathrm{ec,\ max}}$	20	MW	Maximum gyrotron power
w_{sat}	0.32	m	Saturated island width
w_{marg}	0.02–0.06	m	Marginal island width
w_{dep}	0.024	m	Deposition width of ECRH for LSM
$j_{\mathrm{BS}}(r_{\mathrm{s}})$	73×10^{3}	$\mathrm{A\,m^{-2}}$	Bootstrap current at r_{s}
η_{CD}	2.7×10^{-3}	$\mathrm{A\,W^{-1}}$	Current drive efficiency for LSM
$q = m/n$	2/1	—	Safety factor
T_{sep}	5.6	keV	Average electron temperature at separatrix
R_0	6.2	m	Major radius
a	2	m	Minor radius
Z_{eff}	1.7	—	Effective charge
κ	1.7	—	Plasma elongation
r_{s}	1.55	m	Radial location resonant surface
B_{tor}	5.3	T	Toroidal magnetic field
μ_0	$4\pi \times 10^{-7}$	$\mathrm{N\,A^{-2}}$	Vacuum magnetic permeability
$L_q(r_{\mathrm{s}})$	$q/\nabla q = 0.87$	—	Local magnetic shear length
$B_{\mathrm{p}}(r_{\mathrm{s}})$	0.97	T	Poloidal field at the resonant surface
τ_{r}	293	s	Resistive time scale

of the GRE. The ITER scenario 2 is an inductive scenario at 15 MA, with plasma pressure $\beta_{\mathrm{N}} = 1.8$ and plasma self-inductance $l_{\mathrm{i}} = 0.8$ with a burn duration of approximately 400 s [14]. The values for the current drive efficiency η_{CD} and the deposition width of the ECRH/ECCD beam w_{dep} are taken from calculations [24] performed by a beam tracing code, TORBEAM [25], and hold for the lower steering mirror (LSM) of the ITER ECRH/ECCD installation. The ITER major radius $R_0 = 6.2$ m and minor radius $a = 2$ m are given in [6, 14]. The elongation $\kappa = 1.7$ is given in [14]. The toroidal magnetic field B_{tor} for the burning plasma scenario in ITER is $B_{\mathrm{tor}} = 5.3$ T, this value is mentioned in a data-set for ITER scenario 2[Note 3] and in [6, 14]. The radial location of the resonant surface at radius r_{s} is $r_{\mathrm{s}} = 1.55$ m [26] for the $m/n = 2/1$ mode. This radius is half the diameter of the flux surface in the midplane. This differs by a factor $1/\sqrt{\kappa}$ from equivalent cylindrical coordinates, see remarks in [24]. The value for r_{s} corresponds to the value mentioned in [27], where $r_{\mathrm{s}} = 1.53$ m is used. A value for the local magnetic shear at $q = m/n = 2/1$, which is defined as $L_q = q/(\mathrm{d}q/\mathrm{d}r) = 0.87$ m, is taken from [26]. Given these values, the poloidal field at r_{s} can be approximated to be $B_{\mathrm{pol}}(r_{\mathrm{s}}) = (r_{\mathrm{s}} B_{\mathrm{tor}})/(R_0 q)$ or $B_{\mathrm{pol}}(r_{\mathrm{s}}) = 0.97$ T [26]. The bootstrap current near r_{s} in ITER scenario 2 (see footnote 3) is $j_{\mathrm{BS}} = 73.7\,\mathrm{kA\,m^{-2}}$ [24]. Note that [27] uses a value $72\,\mathrm{kA\,m^{-2}}$, where $j_{\mathrm{eccd}}/j_{\mathrm{BS}} = 0.63$ [22]. The global current drive efficiency η_{CD} is derived from the expression [24]

$$\eta_{\mathrm{CD}} P_{\mathrm{ec}} = I_{\mathrm{CD}} \gtrsim \pi^{3/2} \sqrt{\kappa} r_{\mathrm{s}} w_{\mathrm{dep}} j_{\mathrm{CD,max}}, \qquad (10)$$

where $j_{\mathrm{CD,max}}$ is the maximum in the driven current density profile at the mode rational surface. For the LSM of the ITER ECRH/ECCD installation, a value $\eta_{\mathrm{CD}} = 2.7\,\mathrm{kA\,MW^{-1}}$ is found using TORBEAM calculations following [17, 24]. The electron temperature at the separatrix of the magnetic island is assumed to be $T_{\mathrm{sep}} = 5.6$ keV [26]. The width of a saturated island in the ITER scenario is assumed to be $w_{\mathrm{sat}} = 0.32$ m, this value is also used for the 2/1 NTM in [6]. The marginal island width is chosen as $w_{\mathrm{marg}} = 0.02$ m in this work. Reference [6] uses $w_{\mathrm{marg}} \in [0.02, 0.06]$ m. The deposition width of ECRH/ECCD is of the same order of magnitude and can be chosen as $w_{\mathrm{dep}} \in [0.02, 0.03]$ m. The TORBEAM calculation gives a value $w_{\mathrm{dep}} = 0.024$ m for injection via the LSM [24]. The analysis presented in this paper uses $w_{\mathrm{dep}} = 0.024$ m. The resistive time scale from Spitzer resistivity equals $\tau_{\mathrm{r}} = 293$ s for the 2/1 island in ITER scenario 2.

[3] Data-base ITER plasma scenario II (15 MA, inductive) at burn; ASTRA simulation with the boundary conditions from PRETOR code (1999).

4. Equilibria and analysis of system dynamics

4.1. Solution of the GRE

Using the parameter set and assumptions made in the previous sections, solutions of the GRE can be computed for different levels of the applied ECRH/ECCD power P_{ec}. Figure 1 shows such solutions of the NTM growth rate $\mathrm{d}w/\mathrm{d}t$ as a function of the NTM width w and (fixed) values of P_{ec}. The upper black curve is obtained when $P_{\mathrm{ec}} = 0$ MW is applied to the island. A stepwise increase in the ECRH/ECCD power being deposited in the island centre or O-point results in a downward shift of the $\mathrm{d}w/\mathrm{d}t$ versus w curve, as reflected by the subsequently plotted dashed curves in figure 1.

4.2. Numerical analysis of the equilibria of the equation

We will now first investigate the properties of the system, without ECRH/ECCD, i.e. with $P_{\mathrm{ec}} = 0$. This corresponds with the black solid curve in figure 1. $P_{\mathrm{ec}} = 0$ trivially implies that $r_{\mathrm{s}} \Delta'_{\mathrm{CD}} = 0$. Using the parameter set specified in table 1, the terms in the GRE can be written as explicit numerical values. The equation then reads

$$\frac{\mathrm{d}w}{\mathrm{d}t} = -0.0143 + 11.5 \cdot w/(2500w^2 + 1). \qquad (11)$$

By choosing $\mathrm{d}w/\mathrm{d}t = 0$ and solving the resulting expression, the equilibria or zeros of this differential equation can be computed. Two equilibria are found, which have very different properties: $w_1 = 0.32$ m is a stable equilibrium usually referred to as the saturated island width w_{sat}. This equilibrium point is stable since $\mathrm{d}w/\mathrm{d}t < 0$ for $w > w_1$ and close to w_1, and $\mathrm{d}w/\mathrm{d}t > 0$ for $w < w_1$ and close to w_1. Similarly it can be concluded that the other equilibrium, $w_2 = 0.001\,25$ m, is unstable. In fact, for $P_{\mathrm{ec}} = 0$ it holds that the region of attraction of w_1 is given by (w_2, w_{sat}), meaning that when $w(t = 0) \in (w_2, w_{\mathrm{sat}})$, the corresponding solution eventually

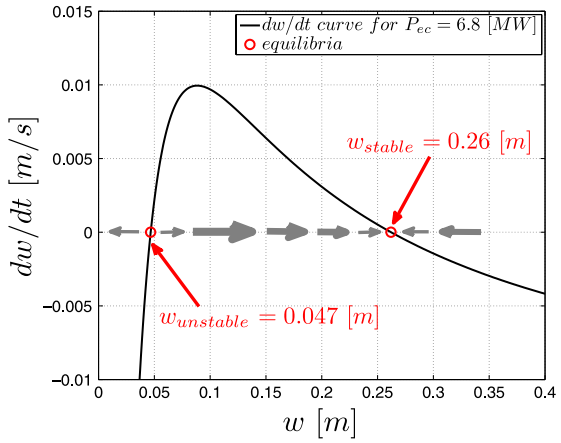

Figure 2. Phase diagram of the GRE plotted as $\mathrm{d}w/\mathrm{d}t$ versus w for the case when 6.8 MW of ECRH/ECCD is applied to the $m/n = 2/1$ NTM to suppress the mode. Two equilibria are found, one stable equilibrium at $w_1 = 0.26$ m and an unstable equilibrium at $w_2 = 0.047$ m. Unstable equilibria are typically found when a sufficient amount of power is applied to bring the island width below w_{thres}. The solid black curve is the solution of the GRE for $P_{\mathrm{ec}} = 6.8$ MW. The direction of the velocity vector near the two equilibria is indicated by the grey arrows, representing the phase portrait of the system. The goal of the feedback controllers derived in this paper is to stabilize the unstable equilibrium w_{unstable}, which lies below w_{thres}.

converges to w_1, i.e. $\lim_{t\to\infty} w(t) = w_1$. The second equilibrium denotes a critical island width $w_2 = w_{\mathrm{crit}} = w_{\mathrm{unstable}} = 0.001\,25$ m below which the island dynamics cause the island to suppress completely. NTMs are usually termed to be meta-stable in the sense that they are linearly stable, but unstable at finite w. Note that although $w = 0$ is a stable equilibrium for NTMs, it is not explicitly found as an equilibrium of the GRE.

We will now consider the effect of the application of ECRH/ECCD to the system, i.e. $P_{\mathrm{ec}} > 0$. We only consider the case of power deposition when $r_{\mathrm{dep}} = r_{\mathrm{s}}$, i.e. the applied ECRH/ECCD is properly aligned with the rational surface at which the island resides. The resulting equilibria can be computed for constant P_{ec} using the GRE which now reads

$$\frac{\mathrm{d}w}{\mathrm{d}t} = -0.0143 + 0.0046w/(w^2 + 1/2500) - 1.2\times 10^{-7} P_{\mathrm{ec}} N_{\mathrm{CD}} \left(w/w_{\mathrm{dep}}\right). \quad (12)$$

Again, by setting $\mathrm{d}w/\mathrm{d}t = 0$ and solving the resulting expression, the equilibria of the differential equation can be computed in a straightforward manner.

As an example, we consider a case with $P_{\mathrm{ec}} = 6.8$ MW. The equilibria are now computed by substitution of $P_{\mathrm{ec}} = 6.8$ MW and $\mathrm{d}w/\mathrm{d}t = 0$ in expression (12) and solving for w. The real positive solutions of (12) with $\mathrm{d}w/\mathrm{d}t = 0$ are now $w_1 = 0.26$ m and $w_2 = 0.047$ m. Figure 2 shows a phase portrait for the case when $P_{\mathrm{ec}} = 6.8$ MW is applied to the 2/1 island. The island dynamics represented in this phase portrait show the two equilibria. From the sign of $\mathrm{d}w/\mathrm{d}t$ near the equilibria it is clear that $w_1 = w_{\mathrm{stable}}$ is a stable equilibrium and w_2 is an unstable equilibrium.

As shown in figure 1, the threshold island width w_{thres} corresponds to the island width which is achieved for the minimal value of the applied ECRH/ECCD power P_{ec} for which $\mathrm{d}w/\mathrm{d}t$ is always smaller or equal 0, i.e. $\mathrm{d}w/\mathrm{d}t \leqslant 0$ for all $w \geqslant 0$. In figure 1, it is shown that $\mathrm{d}w/\mathrm{d}t \leqslant 0$ for all w, which is reached when applying $P_{\mathrm{ec}} \approx 11.47$ MW of ECRH/ECCD power, resulting in a threshold island width $w_{\mathrm{thres}} \approx 0.158$ m. The power level corresponding with this threshold will be denoted as $P_{\mathrm{ec,\ Wthres}}$ in the rest of this work. From the solutions it is clear that a stable island width can always be found above an island width $w > w_{\mathrm{thres}}$ (figure 1). This implies that NTMs of considerable size above the threshold island width w_{thres} can be (locally) stabilized in open loop, i.e. using constant values of P_{ec}. Below $w = w_{\mathrm{thres}}$, the phase portrait shows a negative growth rate of the island. Open-loop stabilization of islands for $w < w_{\mathrm{thres}}$ is unfeasible.

4.3. Control goal

We will now show in simulation that an island's size can be stabilized in the domain $w_{\mathrm{crit}} < w < w_{\mathrm{sat}}$ by applying a closed-loop control strategy. In order to close the feedback loop, first, it is assumed that the island width is known or measured accurately. Second, a certain desired, constant island width w_{ref} is specified, which serves as the reference signal in the control loop. Next, the island width is fed back from the system output and a control error $e = w - w_{\mathrm{ref}}$ is constructed. A controller is now designed and implemented with the objective to stabilize the island size at any w_{ref} in the domain $w_{\mathrm{crit}} < w_{\mathrm{ref}} < w_{\mathrm{sat}}$ meaning that the control error e should converge to $e \approx 0$. For this purpose we will first consider a classical linear controller, subsequently followed by two nonlinear controllers.

5. Classical linear controller

In the design of a controller for the stabilization of the NTM width below w_{thres} we start with the design of a linear feedback controller. First observe that the GRE (1) takes the form of a nonlinear ordinary differential equation (ODE) [20]

$$\dot{x} = f(x,u), \quad (13)$$

$$y = x, \quad (14)$$

where $x \equiv w \in \mathbb{R}^+$ is the state, with $\mathbb{R}^+$ the set of nonnegative reals, i.e. $\mathbb{R}^+ = [0,\infty)$ and $u \equiv P_{\mathrm{ec}} \in \mathbb{R}^+$ is the input. $y \equiv w = x \in \mathbb{R}^+$ is the output, f is a function and $\dot{x} \equiv \mathrm{d}x/\mathrm{d}t \equiv \mathrm{d}w/\mathrm{d}t$. Note that both x and y as well as u are nonnegative.

In particular, in our setup, expression (13) can be written as

$$\dot{x} = f(x,u) = g(x) + h(x)u, \quad (15)$$

where the original function $f(x,u)$ as given by the GRE is now split into two separate parts $g(x)$ and $h(x)u$ with

$$g(x) = \frac{r_{\mathrm{s}}}{0.82\tau_{\mathrm{r}}}\frac{16\mu_0 L_q r_{\mathrm{s}}}{B_{\mathrm{p}}\pi} \times \left(-\frac{4}{3w_{\mathrm{sat}}}\frac{w_{\mathrm{sat}}^2}{w_{\mathrm{sat}}^2 + w_{\mathrm{marg}}^2} j_{\mathrm{BS}} + \frac{4}{3}\frac{x}{x^2 + w_{\mathrm{marg}}^2} j_{\mathrm{BS}}\right), \quad (16)$$

$$h(x) = -\frac{r_{\mathrm{s}}}{0.82\tau_{\mathrm{r}}}\frac{16\mu_0 L_q}{B_{\mathrm{p}}\pi}\frac{\eta_{\mathrm{cd}}}{w_{\mathrm{dep}}^2} \times \frac{0.25 + 0.24\left(\frac{x}{w_{\mathrm{dep}}}\right)}{1 + 0.64\left(\frac{x}{w_{\mathrm{dep}}}\right)^3 + 0.43\left(\frac{x}{w_{\mathrm{dep}}}\right)^2 + 1.5\left(\frac{x}{w_{\mathrm{dep}}}\right)}. \quad (17)$$

As we will see, the definition of the functions $g(x)$ and $h(x)$ is useful for later purposes. When implementing a feedback controller on the system (13)–(14), the input u is replaced by a feedback law. We first propose a basic controller consisting of classical proportional and integral actions (PI). Note that principally, the first-order system (13)–(14) can be stabilized by feedback control in a single operating point with a simple proportional gain controller. The integral action, however, is incorporated for reduction of the steady-state error, which is of importance as the specified control objective is to guarantee convergence of x to the setpoint w_{ref}. The PI controller takes the form

$$u = -k_1 e - k_2 \sigma, \tag{18}$$

where k_1 is the proportional gain, $e = x - w_{\mathrm{ref}} = w - w_{\mathrm{ref}}$ is the control error, σ is the integrated error $\sigma = \int e\,\mathrm{d}t$ that can be obtained by integration of the expression $\dot{\sigma} = e$ and k_2 is the integrator gain. Using this control law, the closed-loop system constituted by combination of (13) and (18), can be written as

$$\dot{x} = f(x, -k_1 e - k_2 \sigma) = \xi(x, \sigma), \tag{19}$$

$$\dot{\sigma} = e = x - w_{\mathrm{ref}}, \tag{20}$$

where a new function $\xi(x, \sigma) = f(x, -k_1 e - k_2 \sigma) = f(x, -k_1 x + k_1 w_{\mathrm{ref}} - k_2 \sigma)$ has been introduced.

The qualitative behaviour of the feedback controlled nonlinear system (19)–(20) near an operating point can be analysed by computing a linearization of (19)–(20). The setpoint w_{ref} is a good choice as an operating point for the linearization. This linearization can be obtained by computing the equilibrium $(\bar{x}, \bar{\sigma})^T$ corresponding to w_{ref}, i.e. the value of $(\bar{x}, \bar{\sigma})^T$ such that

$$\dot{x} = \xi(\bar{x}, \bar{\sigma}) = 0, \tag{21}$$

$$\dot{\sigma} = \bar{x} - w_{\mathrm{ref}} = 0, \tag{22}$$

$$y = \bar{x} = w_{\mathrm{ref}}. \tag{23}$$

Hence, $\bar{x} = w_{\mathrm{ref}}$ and $\bar{\sigma}$ follows from $\xi(\bar{x}, \bar{\sigma}) = 0$. Note that when the system (19) and (20) is in the equilibrium it holds that $u = \bar{u} \equiv -k_2 \bar{\sigma}$ as $e = \bar{x} - w_{\mathrm{ref}} = 0$. Next it is analysed how a small perturbation of the equilibrium $\sigma = \bar{\sigma} + \tilde{\sigma}$ and $x = \bar{x} + \tilde{x}$ affects the system through a linearization of the closed loop (19) and (20).

5.1. Linearization

In order to study the stability of an equilibrium $(\bar{x}, \bar{\sigma})^T$ for the feedback controlled system (19) and (20) given a certain choice of the controller gains k_1 and k_2, linearizations are usually performed near the specific equilibrium point. To do so, the expression of the GRE in the form (19) is now linearized. Using the above expressions, the ODE (19) is rewritten as [20]

$$\dot{\tilde{x}} = \dot{x} = \xi(x, \sigma) = \xi(\bar{x} + \tilde{x}, \bar{\sigma} + \tilde{\sigma}), \tag{24}$$

which can be linearized when the function ξ is continuously differentiable. Since this is the case for the GRE when $w > 0$, the right-hand side of the GRE is now expanded in its Taylor series near the equilibrium point $(\bar{x}, \bar{\sigma})^T$. Making use of the Jacobians $\partial\xi/\partial x$ and $\partial\xi/\partial\sigma$, the Taylor series expansion yields

$$\dot{\tilde{x}} = \underbrace{\xi(\bar{x}, \bar{u})}_{=0} + \left.\frac{\partial \xi}{\partial x}\right|_{(\bar{x},\bar{\sigma})^T} \tilde{x} + \left.\frac{\partial \xi}{\partial \sigma}\right|_{(\bar{x},\bar{\sigma})^T} \tilde{\sigma} + \mathrm{H.O.T.}, \tag{25}$$

where H.O.T. denotes the higher-order terms of the Taylor series expansion. The higher-order terms can be neglected if the linearization is restricted to a sufficiently small area around the equilibrium point $(\bar{x}, \bar{\sigma})^T$.

The Taylor expansion is thus used to approximate the nonlinear state equation (19) by the linear state-space description

$$\dot{\tilde{x}} = \left.\frac{\partial \xi}{\partial x}\right|_{(\bar{x},\bar{\sigma})^T} \tilde{x} + \left.\frac{\partial \xi}{\partial \sigma}\right|_{(\bar{x},\bar{\sigma})^T} \tilde{\sigma}. \tag{26}$$

To obtain the partial derivatives $\left.\frac{\partial \xi}{\partial x}\right|_{(\bar{x},\bar{\sigma})^T}$ and $\left.\frac{\partial \xi}{\partial \sigma}\right|_{(\bar{x},\bar{\sigma})^T}$, we first compute the derivative of the function $\xi(x, \sigma)$ with respect to the state x:

$$\left.\frac{\partial \xi}{\partial x}\right|_{(\bar{x},\bar{\sigma})^T} = \left.\frac{\partial f}{\partial x}\right|_{(\bar{x},\bar{u})^T} + \left.\frac{\partial f}{\partial u}\right|_{(\bar{x},\bar{u})^T} \frac{\partial u}{\partial x}, \tag{27}$$

$$= \left.\frac{\partial f}{\partial x}\right|_{(\bar{x},\bar{u})^T} - k_1 \left.\frac{\partial f}{\partial u}\right|_{(\bar{x},\bar{u})^T}. \tag{28}$$

Secondly, the derivative of the function $\xi(x, \sigma)$ with respect to σ is computed:

$$\left.\frac{\partial \xi}{\partial \sigma}\right|_{(\bar{x},\bar{\sigma})^T} = \left.\frac{\partial f}{\partial u}\right|_{(\bar{x},\bar{u})^T} \frac{\partial u}{\partial \sigma} = -k_2 \left.\frac{\partial f}{\partial u}\right|_{(\bar{x},\bar{u})^T}. \tag{29}$$

For the GRE, the derivatives $\partial f/\partial x$ and $\partial f/\partial u$ are given by

$$A \equiv \left.\frac{\partial f}{\partial x}\right|_{(\bar{x},\bar{u})^T} = \left.\frac{\partial g}{\partial x}\right|_{(\bar{x},\bar{u})^T} + \left.\frac{\partial h}{\partial x}\right|_{(\bar{x},\bar{u})^T} \cdot \bar{u} = -C_2 \frac{\left(\bar{x}^2 + w_{\mathrm{marg}}^2\right)}{\left(\bar{x}^2 + w_{\mathrm{marg}}^2\right)^2}$$

$$-C_3 \bar{u} \left(\frac{0.24}{w_{\mathrm{dep}} \left(1 + 0.64 \left(\frac{\bar{x}}{w_{\mathrm{dep}}}\right)^3 + 0.43 \left(\frac{\bar{x}}{w_{\mathrm{dep}}}\right)^2 + 1.5 \frac{\bar{x}}{w_{\mathrm{dep}}}\right)} \right)$$

$$+C_3 \bar{u} \left(\frac{\left(0.25 + 0.24 \frac{\bar{x}}{w_{\mathrm{dep}}}\right) \left(1.92 \left(\frac{\bar{x}}{w_{\mathrm{dep}}}\right)^2 + 0.86 \left(\frac{\bar{x}}{w_{\mathrm{dep}}}\right) + \frac{1.5}{w_{\mathrm{dep}}}\right)}{\left(1 + 0.64 \left(\frac{\bar{x}}{w_{\mathrm{dep}}}\right)^3 + 0.43 \left(\frac{\bar{x}}{w_{\mathrm{dep}}}\right)^2 + 1.5 \frac{\bar{x}}{w_{\mathrm{dep}}}\right)^2} \right), \tag{30}$$

and

$$B \equiv \left.\frac{\partial f}{\partial u}\right|_{(\bar{x},\bar{u})^T}$$

$$= -C_3 \frac{0.25 + 0.24 \left(\frac{\bar{x}}{w_{\mathrm{dep}}}\right)}{1 + 0.64 \left(\frac{\bar{x}}{w_{\mathrm{dep}}}\right)^3 + 0.43 \left(\frac{\bar{x}}{w_{\mathrm{dep}}}\right)^2 + 1.5 \left(\frac{\bar{x}}{w_{\mathrm{dep}}}\right)}. \tag{31}$$

Now that (19) has been linearized, we only have to linearize (20). This is straightforward and leads to $\dot{\tilde{\sigma}} = \dot{\sigma} = e = x - \bar{x} = \tilde{x}$. We now introduce a new variable $\tilde{z} = (\tilde{x}, \tilde{\sigma})^T = (x - \bar{x}, \sigma - \bar{\sigma})^T$, which is used to rewrite the linearized closed-loop system conveniently in the following *state-space form*:

$$\dot{\tilde{z}} = (\mathcal{A} - \mathcal{B}\mathcal{K})\,\tilde{z}, \tag{32}$$

with

$$\mathcal{A} = \begin{bmatrix} A & 0 \\ 1 & 0 \end{bmatrix}, \qquad \mathcal{B} = \begin{bmatrix} B \\ 0 \end{bmatrix}, \qquad \mathcal{K} = [k_1 \;\; k_2],$$

where A and B are given by (30) and (31), respectively.

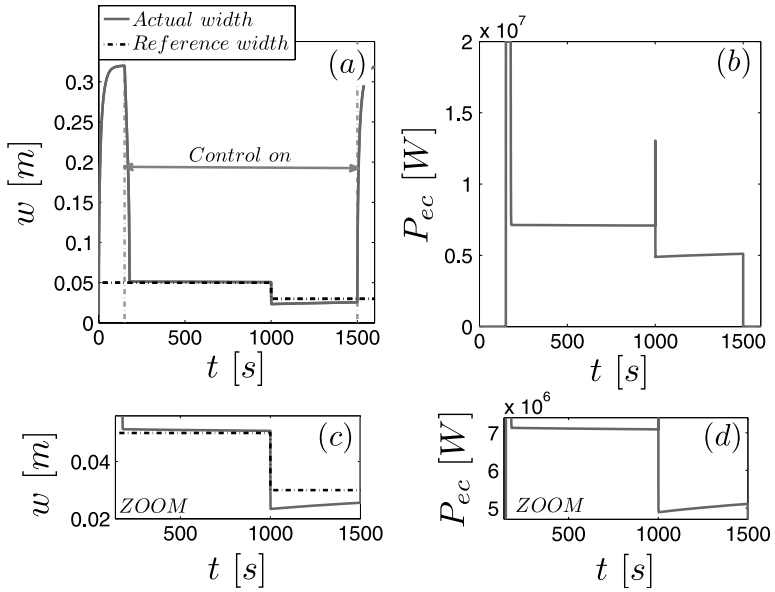

Figure 3. Closed-loop results for a basic PI linear NTM controller. (*a*) depicts the width of the NTM as a function of time. (*b*) depicts the applied ECRH/ECCD power P_{ec} as a function of time. (*c*) and (*d*) show zooms of the island width and ECRH/ECCD power, respectively. As reflected by the results, the control action is initiated at $t = 150$ s whereas the feedback path is opened again at $t = 1500$ s. Stabilization of the island near $w_{\mathrm{ref}} = 0.05$ m with a small error is reached within 30 s after initialization of the control action. Next the integrator action of the controller reduces the error further. As soon as w_{ref} is changed to 0.03 m, at $t = 1000$ s, the applied ECRH/ECCD power peaks during 3 s, the island width remains stabilized, but the error is now larger. The integrator action subsequently reduces the error again. This indicates that the PI controller provides locally appropriate control performance, but this performance is setpoint dependent.

5.2. Closed-loop performance and stability

With the linearization of the closed-loop model completed, the local stability of the closed-loop system (19) and (20) can now be assessed. Indeed, we will discuss next how the control parameter settings for the linear controller can be chosen to provide local stability and control performance results. Using a control design method such as loop-shaping [28] one can design k_1 and k_2 such that the equilibrium $(\bar{x}, \bar{\sigma})^T$ of (19) and (20) is locally stable, which comes down to choosing $\mathcal{K}$ in (32) such that $\mathcal{A} - \mathcal{B}\mathcal{K}$ is Hurwitz stable [20], that is, the eigenvalues λ_1 and λ_2 of $\mathcal{A} - \mathcal{B}\mathcal{K}$ must lie in the open left half of the complex plane, $\mathrm{Re}(\lambda_i) < 0$, $i = 1, 2$ [20]. The controller gains are chosen to optimize the settling behaviour of the feedback controlled system.

As an example, we consider a PI controller with the aim to stabilize an $m/n = 2/1$ NTM at a steady-state width $\bar{x} = w_{\mathrm{ref}} = 0.05$ m. To do so, a reference NTM width $w_{\mathrm{ref}} = 0.05$ m is provided as a setpoint to the control loop. Using the control gains $k_1 = -3 \times 10^8$ and $k_2 = -16 \times 10^4$, local stability is obtained since the eigenvalues of $\mathcal{A} - \mathcal{B}\mathcal{K}$ are now $\lambda_1 = -5.71$ and $\lambda_2 = -3 \times 10^{-4}$. The dynamic behaviour of the system in terms of settling time could be improved by increasing the controller gains such that λ_2 becomes more negative; however, the increase in the controller gain comes at the cost of saturation of the controller output. Note that this stability result is only valid locally, near $w_{\mathrm{ref}} = 0.05$ m. For a given PI controller, one can thus analyse for any w_{ref} whether the reference value is stabilized locally or not.

5.3. Closed-loop simulation

The controlled system is simulated. The closed-loop result is depicted in figure 3. As shown in figure 3, after the control loop is closed at $t = 150$ s, the island width is suppressed within 30 s to an island size close to $w = 0.05$ m. These 30 s correspond to the minimal required time to suppress a fully saturated 2/1 island from its saturated size w_{sat} to $w_{\mathrm{ref}} = 0.05$ m. Note that this suppression rate is determined by the maximally applicable P_{ec} (20 MW). In this phase of the suppression, the controller output is saturated and therefore the behaviour seen in this period is not characteristic for the linear PI controller. However, as soon as the island width approaches the reference the behaviour of the control system becomes linear again. The remaining error after the initial suppression is reduced subsequently by the integrator action of the PI controller in order to converge to the desired setpoint value $w_{\mathrm{ref}} = 0.05$ m and realize $e = w - w_{\mathrm{ref}} \approx 0$. In the feedback scheme no dedicated anti-windup compensation has been applied. Since the integrator term is chosen sufficiently small, the windup effect is negligible. For simulation purposes a saturation limit on the controller output equal to the maximum applicable gyrotron power was set.

Note that the closed-loop performance in terms of convergence speed to the setpoint of the controlled system as shown here can be guaranteed only locally, since the linearization is valid only near $w_{\mathrm{ref}} = 0.05$ m (and σ near $\bar{\sigma}$). Indeed, for small excursions around $w = 0.05$ m and other setpoints w_{ref} close to 0.05 m, the system performance will remain acceptable, but if these deviations become larger or if a different reference NTM width w_{ref} is chosen, convergence to the reference value is no longer guaranteed. In order to demonstrate this, at $t = 1000$ s in the simulation shown in figure 3, the reference width w_{ref} is switched from $w_{\mathrm{ref}} = 0.05$ m to $w_{\mathrm{ref}} = 0.03$ m. The designed controller is able to stabilize the NTM at both setpoint widths, i.e. the island size remains stabilized also when switching to the reference width

of 0.03 m. Although the island width is stabilized near the desired reference, the decrease in the error to zero requires more time than observed for the previous setpoint value. The convergence speed of the controlled system to the setpoint value is clearly setpoint dependent, for this linear controller. This is logical since the controller gains are constant and the linear controller is now applied to stabilize a different setpoint than the one for which it was designed. In fact, another linearized model then describes the local behaviour (of the dependences of A and B in (30) and (31) on $\bar{x} = w_{\text{ref}}$). Hence, the actual island suppression process is clearly nonlinear in nature.

From the local stability results obtained here it has become clear that the inherently unstable NTM width, which normally tends to go to zero below w_{thres} without active control, can now be stabilized locally at a reference width w_{ref} in the domain $w_{\text{crit}} < w_{\text{ref}} < w_{\text{thres}}$ by a stabilizing linear feedback controller. From the viewpoint of the steady-state operation of a tokamak it would be highly desirable to extend these local results to a broader operational domain. The PI controller provides satisfactory setpoint tracking only in a limited region around a particular reference point w_{ref}, as discussed previously. Given the nonlinear nature of the NTM stabilization problem, the gains of the PI controller appear to be less effective for operating points different from the one for which the controller has been derived. Note that the local results of the PI controller can be extended to the domain $w_{\text{crit}} < w_{\text{ref}} < w_{\text{sat}}$ using adaptive techniques such as gain scheduling or by the inclusion of an anti-windup compensation [20]. As a natural next step, we will therefore proceed to design a controller, which aims at reaching global stability, good control performance and setpoint tracking with negligible overshoots over the entire domain of operation, i.e. for all $w_{\text{ref}} \in (w_{\text{crit}}, w_{\text{sat}})$. Nonlinear feedback controllers are therefore considered next. In particular, we first consider a sliding mode or switching controller [19, 20], while later in section 7, we consider a linearizing feedback approach [20].

6. Sliding mode controller

It is clear from the analysis of the dynamics of the island evolution that the problem which we are studying is nonlinear in nature. Given the nonlinearity of the island dynamics a more straightforward choice would be to use a nonlinear control law. The aim would then be to allow good convergence to the setpoint for a wider operation range than just one operating point.

To realize convergence to the setpoint, the control error which was defined as $e \equiv y - w_{\text{ref}} = x - w_{\text{ref}}$ should vanish. A straightforward choice for a nonlinear feedback control strategy would be to increase the power level of the applied ECRH/ECCD just above $P_{\text{ec, }w_{\text{thres}}}$ when $e > 0$ (as then $\mathrm{d}w/\mathrm{d}t < 0$ for all $w \in (w_{\text{crit}}, w_{\text{sat}})$), while decreasing the power level when $e < 0$. The desired control behaviour could, for example, be achieved by a simple switching logic, such as

$$u = \begin{cases} P_- & \text{for } e \leqslant 0, \\ P_+ & \text{for } e > 0. \end{cases} \tag{33}$$

A nonlinear controller of the form (33) is a typical example of a sliding mode controller [19, 20]. Two switching levels are defined in this switching logic, notably P_+ and P_-. We choose the high power level of the switching rule $P_+ > P_{\text{ec}}, w_{\text{thres}}$, which guarantees island suppression with $\mathrm{d}w/\mathrm{d}t < 0$ for all $w \in \mathbb{R}^+$. To choose P_+, one should take into account that the convergence speed of an implementation of the switching logic in a reference tracking setup is directly related to the value chosen for P_+. In the choice of the value for P_+ one should make a trade-off between desired convergence speed and practically feasible power levels. To choose the lower level P_- of the switching rule, one should realize that given a certain desired reference width w_{ref}, the choice of P_- determines if w_{ref} can be stabilized at the desired value. That is, P_- should be chosen such that $w_{\text{ref}} \in (w_{\text{unstable}}(P_-), w_{\text{sat}})$, where $w_{\text{unstable}}(P_-)$ is the unstable island width as indicated in figure 2 corresponding to a selected ECRH/ECCD power P_-. For a given value of P_-, $w_{\text{unstable}}(P_-)$ determines the smallest island width for which it is guaranteed that if $w < w_{\text{ref}}$, that $\mathrm{d}w/\mathrm{d}t > 0$. The corresponding region of attraction of the controlled system is then given by $w(0) \in (w_{\text{unstable}}(P_-), w_{\text{sat}})$. The choice of P_- thus determines the region of attraction for which island stabilization is possible. By lowering the power level, the region of attraction for w_{ref} is extended. The largest region of attraction is obtained by selecting the lower level P_- as 0 MW. Note, however, that islands smaller than the critical island width $w_{\text{crit}} = 0.00125$ m cannot be stabilized. Hence, the largest region of attraction is $(w_{\text{crit}}, w_{\text{sat}})$. In general, P_- is selected sufficiently small such that first the desired w_{ref} is indeed locally stabilized (i.e. $w_{\text{ref}} \in (w_{\text{unstable}}(P_-), w_{\text{sat}})$ and second the region of attraction $(w_{\text{unstable}}(P_-), w_{\text{sat}})$ is sufficiently large. One should take into account that the practical implementation of switching between high values of P_+ and low values of P_- on a gyrotron is limited by actuator constraints.

6.1. Closed-loop simulation

As an example, we arbitrarily choose as the lower level $P_- = 6.8$ MW and as the higher level $P_+ = 11.9$ MW. Applying 6.8 MW of ECRH/ECCD power to the island would in open loop result in an unstable island size of $w_{\text{unstable}}(P_-) = 0.047$ m, which corresponds with the value as given in figure 2. The region of attraction for any setpoint $w_{\text{ref}} \in (0.047, w_{\text{sat}})$ for this sliding mode controller is thus given by $(0.047, w_{\text{sat}})$. Any island below $w_{\text{unstable}} = 0.047$ m cannot be stabilized by the chosen settings of the switching law (33).

The resulting closed-loop behaviour for the sliding mode controller (33) is depicted in figure 4 again for a setpoint $w_{\text{ref}} = 0.05$ m which switches to $w_{\text{ref}} = 0.03$ m at $t = 1000$ s. Figure 4(*a*) represents the width of the NTM as a function of time. Note that the island grows to its saturated width $w_{\text{sat}} = 0.32$ m in the time interval from 0 to 150 s when no ECRH/ECCD is applied ($P_{\text{ec}} = 0$ MW). At $t = 150$ s, the sliding mode controller (33) is switched on again with the control objective to stabilize the island at $w_{\text{ref}} < w_{\text{thres}}$. From time $t = 1000$ s on, we choose to stabilize the setpoint $w_{\text{ref}} = 0.03$ m. Figure 4(*b*) shows the resulting actuation signal of the gyrotron power P_{ec}. Note that the switching law first keeps the applied ECRH/ECCD power constant at the power level $P_{\text{ec}} = 11.9$ MW, as long as $w > w_{\text{ref}}$. As soon

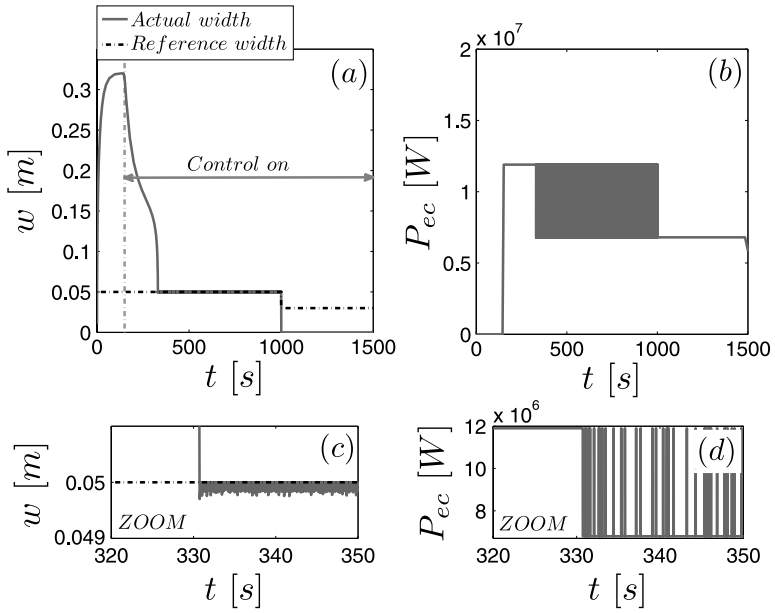

Figure 4. Closed-loop results for a nonlinear sliding mode NTM controller. (*a*) depicts the width of the NTM as a function of time. (*b*) depicts the applied ECRH/ECCD power P_{ec} as a function of time. (*c*) and (*d*) show zooms of the island width and ECRH/ECCD power, respectively. As reflected by the results, the control action is initiated at $t = 150$ s whereas the feedback path is opened again at $t = 1500$ s. $P_- = 6.8$ MW and $P_+ = 11.9$ MW are used in this simulation. With these settings, the region of attraction is $(0.047, w_{sat})$. Stabilization of the island at $w_{ref} = 0.05$ m is reached within 180 s. As soon as w_{ref} is changed to 0.03 m (outside the region of attraction), the island width is not stabilized any longer and the mode consequently suppresses completely.

as the island width is close to the desired reference value, i.e. $w \approx w_{ref}$, the controller output P_{ec} starts to switch according to the simple switching logic in equation (33). Figures 4(*c*) and (*d*) show zooms of the island width and ECRH/ECCD power, respectively. The results show that the closed-loop switching controller is able to stabilize the mode width at $w = 0.05$ m within 180 s after the activation of the control action.

As reflected in the figure, the switching behaviour results in chattering in the controller output. Note that an asymmetric ripple in w is observed. The occurrence of this ripple can be understood by realizing that the island growth mechanism can only be actuated in the positive direction by the gyrotron. In order to stay at a certain setpoint, the EC power is first raised to the highest level of the switching law of the sliding mode controller. This power level is always larger than the power which is required to keep the island at the same size in a steady-state situation. The switching law thus causes a small overshoot on w. As soon as $e = w - w_{ref}$ is smaller or equal than zero, the switching law switches to the lower level. The feedback system then relies on the growth dynamics of the island itself to drive the island width back to the reference value. This causes the asymmetric ripple in w which after averaging results in a steady-state error, as observed in the figure.

Given the settings for the power levels in (33), the closed-loop result for the controller settings chosen here is only stable for operating points larger than $w_{unstable} = 0.047$ m. This can be clearly observed in the simulation, see figure 4. When changing the reference width to $w_{ref} = 0.03$ m, the mode width cannot be stabilized at the reference value anymore and consequently suppresses completely. Note that by decreasing the lower power level P_- in the switching law, the island width can be stabilized at $w_{ref} = 0.03$ m as well and the region of attraction of the controller can be extended. The required time for suppression can be reduced by selecting a higher value for the power level P_+. For $P_+ = 20$ MW, the island width would still be stabilized at $w = 0.05$ m but with a similar convergence speed to the setpoint as the other controllers presented in this paper.

The design principles and simplicity of the sliding mode controller make this controller attractive. The simulations show its effectiveness. The functioning of the controller is rather intuitive, but the main drawback for a practical implementation of this controller is related to the chattering of the controller output P_{ec} between the values P_+ and P_-, which results in a very high control activity and demands fast switching of the gyrotron power as shown in the simulation results. Although methods are available to limit the amount of chattering [19], by including some hysteresis effects in (33), the gyrotron producing the ECRH/ECCD power in practice should still be able to execute high frequent switching over a large power range, which might be undesirable.

7. Feedback linearizing controller

As an alternative nonlinear controller, which also aims at global convergence to the requested setpoint values, a feedback linearizing control law is now introduced. For the design of a feedback linearizing control law, the GRE is again written as

$$\dot{x} = g(x) + h(x)u, \tag{34}$$

with the nonlinear terms $g(x)$ and $h(x)$ as defined earlier in the expressions (16) and (17). The goal of feedback linearization [20] is to design a control law u such that a nonlinear system of the form (34) is transformed from a nonlinear system into a linear system with a new controller output. Given

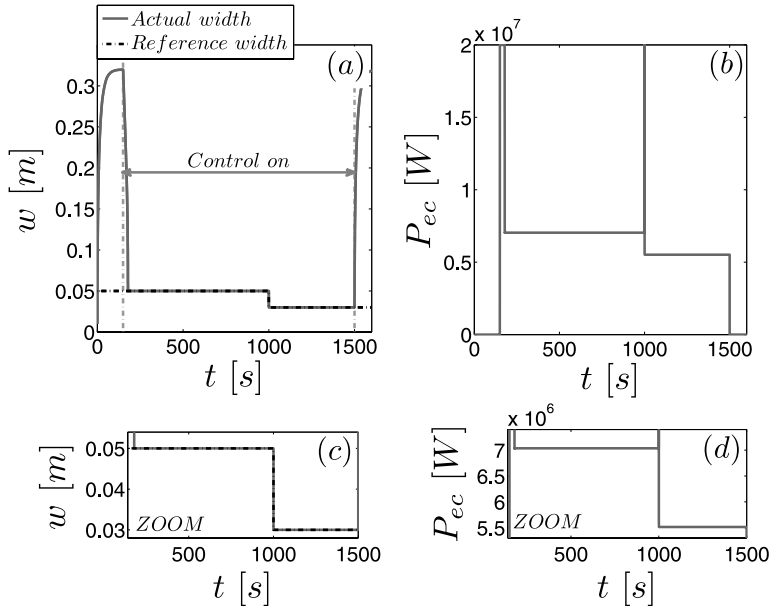

Figure 5. Closed-loop results for the feedback linearizing NTM controller. (*a*) depicts the width of the NTM as a function of time. (*b*) depicts the applied ECRH/ECCD power P_{ec} as a function of time. (*c*) and (*d*) show zooms of the island width and ECRH/ECCD power, respectively. As reflected by the results, the control action is initiated at $t = 150\,\mathrm{s}$. Stabilization of the island at $w_{\mathrm{ref}} = 0.05\,\mathrm{m}$ is reached within 30 s after activation of the control law. The steady-state error is zero. As soon as w_{ref} is changed to 0.03 m, the island width remains stabilized, and there is again a steady-state error of zero. The feedback linearizing control law thus provides perfect reference tracking, which is independent of the chosen setpoint.

the nonlinearity of the GRE, feedback linearization can be a suitable strategy for the NTM control problem. Since the GRE is a first-order standard ODE, a feedback linearizing controller can straightforwardly be chosen as

$$u = -\frac{g(x)}{h(x)} + \frac{\nu}{h(x)}, \tag{35}$$

where ν is considered as a new auxiliary controller output. By substitution of this control law u in (34) one can immediately see that

$$\dot{x} = g(x) + h(x)\left(-\frac{g(x)}{h(x)} + \frac{\nu}{h(x)}\right) = \nu. \tag{36}$$

Hence, the feedback law u (35) indeed cancels the nonlinear terms $g(x)$ and $h(x)$, resulting in the linear system $\dot{x} = \nu$. Since we now have a linear system, standard control techniques can be exploited to synthesize a control law for ν. When the input ν is governed by a linear controller, e.g. a proportional gain or a PI controller to render the closed-loop system stable, the resulting closed-loop system is indeed linear.

Here, we choose to use

$$\nu = -Ke, \tag{37}$$

for the auxiliary controller output. Hence, the control law specifying ν is chosen as a standard proportional action, where $\nu = -Ke$ with $e = y - w_{\mathrm{ref}} = x - w_{\mathrm{ref}}$ and $K > 0$ for stability and tracking purposes. The gain K can be used to tune the closed-loop behaviour. Note that the choice of the control law in equations (35) and (37) implies that the steady-state error is zero even without adding an integral term in the control law.

Two remarks are in order on the chosen control strategy. First, instead of a proportional gain one could also use a proportional, integral action, which will probably enhance the performance further. Second, the feedback linearization procedure works in the case that the model matches the real system behaviour adequately as only then (36) is true. If the dynamics of the real system differ from the dynamics governed in the model, the nonlinear terms $g(x)$ and $h(x)$ in (34) are not adequately cancelled. The resulting feedback linearized system then still shows nonlinear behaviour. This implies that the conversion of this control concept into a practically relevant controller requires detailed model knowledge for optimal performance, and given the uncertainties of the GRE in the small island regime, this model knowledge may need to be improved based on experiments.

7.1. Closed-loop simulation

A closed-loop simulation is performed with the feedback linearizing controller. In the control law $\nu = -Ke$, a proportional gain $K = 10$ is used. Again a setpoint $w_{\mathrm{ref}} = 0.05\,\mathrm{m}$ is chosen which switches to $w_{\mathrm{ref}} = 0.03\,\mathrm{m}$ at $t = 1000\,\mathrm{s}$. The result is depicted in figure 5. Stabilization of the island at $w_{\mathrm{ref}} = 0.05\,\mathrm{m}$ is reached within 30 s after activation of the controller. The steady-state error is zero. The same holds when switching the setpoint to $w_{\mathrm{ref}} = 0.03\,\mathrm{m}$.

8. Comparison

In order to compare the three controllers derived and simulated so far, their main features are summarized in table 2. It has been shown that the PI controller, sliding mode controller and the feedback linearizing controller are capable of satisfactory stabilization of islands at small sizes below w_{thres}. When comparing the sliding mode controller and

Table 2. Comparison of the three control concepts.

	PI controller	Sliding mode controller	FB linearizing controller
Type	Linear	Nonlinear	Nonlinear
Region of attraction	'Local'	'Global'	'Global'
Further issues		Chattering	Accurate model needed

feedback linearization controller on the one hand and the PI controller on the other hand, the difference in stabilization between the two nonlinear controllers and the PI controller is significant. Whereas the PI controller managed to stabilize the width of an island locally at w_{ref} with guarantees only for the convergence to the setpoint for which it was designed, the nonlinear controllers guarantee stabilization of the island at any w_{ref} with negligible steady-state error. Note once more that the convergence speed of the feedback controlled system to the setpoint value is limited by the maximum applicable P_{ec} of 20 MW (as is observed in figures 3 and 5). For the sliding mode controller the applicable P_{ec} is also restricted by the desired $w_{\text{min}} = f(P_{-}) > w_{\text{crit}}$.

The PI controller thus offers local stabilization guarantees and local performance, whereas both nonlinear controllers aim at reaching more global setpoint stabilization in a larger operational region. It was already mentioned that in a practical implementation, the local results of the PI controller can be extended using adaptive techniques such as gain scheduling or by the inclusion of an anti-windup compensation [20]. The main drawback of the sliding mode controller in a practical implementation is the high-frequency chattering of the control signal, although some methods are available to reduce the chattering at the costs of introducing steady-state errors [19]. The main disadvantage of effective feedback linearization is the requirement of an accurate model. Any model uncertainty causes deviation from the expected linear model (36) thereby resulting in unexpected behaviour including a non-zero steady-state error. However, this non-zero steady-state error can be compensated for to some extent by adding an integrator part in the control law. This integrator term should be tuned with care since the integrator action might affect the compensation negatively if not tuned correctly.

At this stage of the analysis it is not clear which of the methods would offer the best results as the functionality of the control strategy is strongly dependent on the capabilities of the gyrotrons being used as actuator. However, the presented perspectives and analysis techniques can be used to choose the most optimal control strategy when more information is available on ITER.

9. Considerations for practical implementation

For practical implementation of the linear PI, the sliding mode controller, and the feedback linearizing control techniques discussed in the previous sections, issues related to measurement noise, model (parameter) uncertainty, time delays, saturation and quantization of the applicable gyrotron power should be considered. In particular, the effect of all these issues on the stabilizing properties of the derived

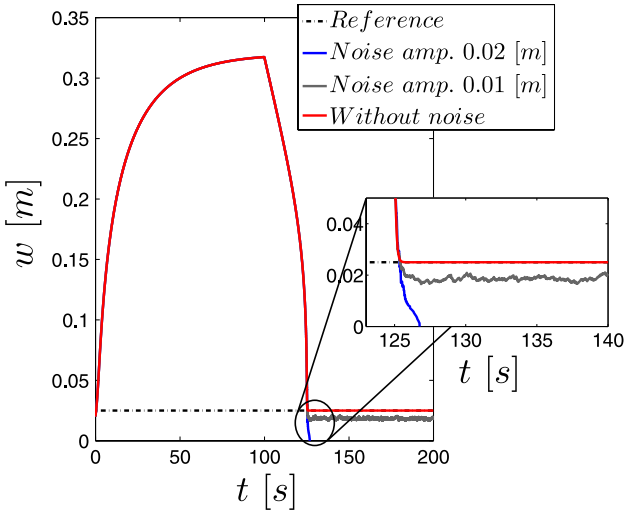

Figure 6. Effect of disturbing noise on the measurement of the island size w. Stabilization of a saturated magnetic island at $w_{\text{ref}} = 0.025$ m is shown for the feedback linearizing controller, where measurement noise is added to the measurement of the island width in the form of random white noise with an amplitude of 1 cm and 2 cm, respectively. For a noise amplitude of 1 cm, the feedback controlled system is still stable, but a sizeable steady-state error exists. A measurement noise amplitude of 2 cm results in an unstable system, for which the magnetic island can not be stabilized at $w_{\text{ref}} = 0.025$ m any longer.

feedback controllers and their robustness must be addressed. Since such an analysis is specifically dependent on the chosen implementation environment, we limit the discussion here to relatively simple simulations of the effect of measurement noise and time delay on the control result. This will indicate that such an analysis is indeed possible.

Suppose the measurement uncertainty on the island width measurement can be represented by random noise with a maximum amplitude of 0.01 m and a uniform distribution, which is added in the simulation by injection of random noise at the system output. Figure 6 shows closed-loop magnetic island stabilization results, where the goal is to stabilize the island at $w_{\text{ref}} = 0.025$ m, using the feedback linearizing controller. As shown in the results, without application of noise, the feedback linearizing controller is able to stabilize the island at the desired width of 0.025 m. When applying noise, the island width remains stabilized but a small steady-state error of 0.005 m remains, which is not compensated for by the control action. Adding an integrator term in the control law v would compensate this steady-state error to a large extent. When the noise amplitude is increased by a factor two, the island width is not stabilized at the reference width anymore but the mode suppresses completely, $w \to 0$. This is a general problem at the small island sizes chosen in the example shown here. As soon as $w < w_{\text{crit}}$, with $w_{\text{crit}} = 0.00125$ m for the model discussed here, w eventually goes to zero, disregarding the control law.

Figure 7 shows island stabilization at a reference width of $w_{\text{ref}} = 0.02$ m using the feedback linearizing control law. A delay term is added to the measurement of the island width, in the feedback path of the controlled system in the simulation. A delay of $\Delta t = 0.05$ s is chosen first. The simulation result in figure 7 for the $\Delta t = 0.05$ s case shows that island stabilization

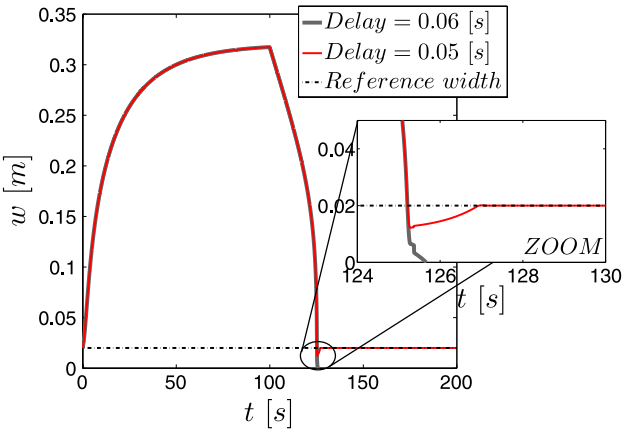

Figure 7. Effect of delay on the closed-loop feedback linearization results. Stabilization of a saturated magnetic island at $w_{\mathrm{ref}} = 0.02$ m is shown for a delay of 0.05 s and 0.06 s in the measurement of the island width, respectively. For a delay of 0.05 s, the feedback controlled system is still stable whereas a delay of more than 0.05 s results in an unstable system. The magnetic island is then not stabilized at $w_{\mathrm{ref}} = 0.02$ m any longer, but suppress completely.

at $w_{\mathrm{ref}} = 0.02$ m is still possible. Increasing the delay to $\Delta t = 0.06$ s again results in an unstable island width, which suppresses completely. Limitation of the time delays in the sensing path is thus important to avoid stability problems, especially if the island size is small and close to w_{crit}. Note that the delay values are chosen arbitrarily, showing in simulation that the system becomes unstable. Generally, for a nonlinear system the influence of time delay on stability is difficult to determine. The effect of time delay on the stability of the reference island width is determined purely with Simulink simulations here. As the time delay threshold for instability will depend on the setpoint w_{ref} and chosen controller gains this has to be checked for each individual case. The time delay threshold for instability found in the simulations presented in figure 7 can therefore not be used for generalization.

10. Pre-emptive closed-loop simulation

Finally, this survey of NTM control strategies is completed by simulation of the pre-emptive closed-loop stabilization of a magnetic island at a small width. Whereas pre-emptive ECRH/ECCD in the literature usually refers to the application of ECRH/ECCD before $t = 0$ to avoid an NTM to grow at all, we use the term pre-emptive slightly different in the sense that we apply closed-loop pre-emptive ECRH/ECCD at $t = 0$ as soon as the island starts to grow. We will restrict the analysis to simulation results obtained using the feedback linearizing control law. ECRH/ECCD is now applied preemptively, in the growth phase of the island before the mode has reached its saturated width w_{sat}. Using the feedback linearizing control law in a closed feedback loop, a mode can be stabilized at a given small island size without ever reaching its saturated island size w_{sat}. Figure 8 shows three simulations in which a 2/1 NTM in ITER is preemptively stabilized at a small island size $w_{\mathrm{ref}} = 0.05$ m. The start of the closed-loop feedback action for each of the three simulations is chosen at a different starting point. When closing the feedback loop at $t = 0$ s, i.e. at the start of the seeding of the NTM, the mode is stabilized at $w = 0.05$ m within 0.6 s. The maximum width never exceeds 0.05 m and the maximum applied ECRH/ECCD power is approximately $P_{\mathrm{ec}} = 7$ MW, which corresponds with the steady-state power level required to stabilize the width at $w = 0.05$ m.

The second simulation shown in figure 8 closes the feedback loop at $t = 2$ s. In the first part of the control experiment, where no control action is applied, the mode grows to a maximum width of $w = 0.10$ m. At $t = 2$ s, the controller is activated and 20 MW of ECRH/ECCD power is immediately applied to the mode. Within 1.4 s, the island is stabilized at $w = 0.05$ m as desired by the reference width tracking controller. The power is then reduced to $P_{\mathrm{ec}} = 7$ MW, resulting in steady-state stabilization of the mode at the desired width. The same experiment is repeated but now closing the feedback loop at $t = 4$ s. The maximum width reached during the simulation is now 0.14 m. Convergence to the setpoint value $w_{\mathrm{ref}} = 0.05$ m takes 3.8 s in this case. At the start of the feedback action $P_{\mathrm{ec}} = 20$ MW is first applied for 3 s. The power setting is later reduced to $P_{\mathrm{ec}} = 7$ MW. Note that the observed difference in island growth rate between the first simulation starting at $t = 0$ s and the other simulation in figure 8 is expected. When the feedback loop is closed at $t = 0$ s, the growth rate is governed by the closed-loop system, i.e. controller and Rutherford equation, whereas for the other simulations, the growth rate is first governed by the Rutherford equation only before the control loop is closed. As shown by the pre-emptive closed-loop results, the required amount of power P_{ec} for stabilization is the lowest for the earliest controller activation. It thus makes sense to start the feedback action as early as possible, preferably in the initial growth phase of the island. In order to close the feedback loop at the right time instant, identifiers for the seeding of the NTM and detectors for mode growth would be required. This further implies that in order for the closed-loop preemptive ECRH/ECCD to be effective (1) the positioning of the ECRH/ECCD deposition with respect to the mode must either be very fast or (2) the ECRH/ECCD launcher system used for this positioning should already be aligned sufficiently accurate with the rational surface at which a mode is expected to occur, before the mode is growing. For fast positioning, a fast steerable launcher system would be required, which uses a dedicated feedback sensor such as line-of-sight ECE [10, 11]. The location of the mode is then determined quickly in the initial growth phase of the island. The second option requires the use of accurate real-time beam tracing and equilibrium reconstruction in the ECRH/ECCD positioning control loop.

11. Conclusions

The designed controllers and corresponding simulation studies and analysis presented in this work show the feasibility of feedback techniques to enable stabilization of small NTM islands in ITER through manipulation of the applied ECRH/ECCD power P_{ec} as a function of the measured island width w. The results in this work demonstrate that it is theoretically possible to adopt such methods to stabilize modes below the threshold island width at which the islands would normally suppress completely if the suppression process was operated in open loop. As a consequence, the

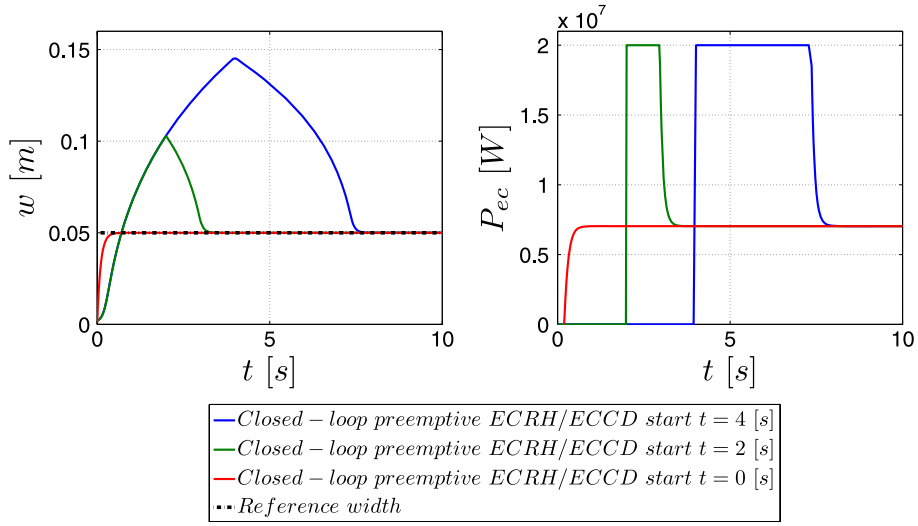

Figure 8. Closed-loop preemptive application of ECRH/ECCD in three simulations. A 2/1 NTM is preemptively stabilized at $w = 0.05$ m in three control simulations where the control action is initiated at three subsequent time instants in the initial growth phase of the island. The feedback linearizing control law is used here.

simulation studies and designs discussed in this paper show the potential for implementation of a NTM control strategy for stabilization of modes at a certain reference width. Obviously, actual experimental implementations of the methods require additional effort, but several considerations in this respect were also discussed in this paper.

A first point of attention for the further development of the NTM control strategies discussed here is related to the detection problem. The width of a magnetic island can be derived from electron cyclotron emission measurements or soft x-ray measurements but the usual diagnostic for estimation of an island's width is provided by the Mirnov coils. In order to isolate the fluctuations corresponding to a certain type of island from the observed magnetic oscillations measured by the coils, several post-processing steps of the data are required. Both the uncertainty in the estimate of the island width as well as the delay caused by the post-processing affect the control performance, as we have shown. In the simulations, the influence of uncertainties and delays was briefly addressed and figures of merit were given for the allowable level of uncertainty and delay in some of the parameters. For a conclusive analysis and a practically implementable controller, the uncertainties and delays should be quantified and taken into account in the design process to optimize the controller design. Of course such analysis cannot be provided at this stage since it is completely dependent on the chosen implementation environment.

In addition to the detection, which should receive more attention, the capabilities of the gyrotrons being used as actuators in the feedback loop also affect the achievable control performance. Based on the simulations, figures of merit can be given for the desired quantization of the ECRH/ECCD power being applied and the speed at which the power level of the gyrotron should be manipulated. The actuator limitations in the form of saturation associated with the minimal and maximal applicable power should also be taken into account when designing a magnetic island width controller for a practical experiment.

Having shown the feasibility and potential of feedback stabilization of the island width, it would be interesting to consider the operational and physical implications, as listed next.

- Stabilization of the mode at a small width would enable the investigation of the validity of the GRE at small island widths and can be used to validate the terms governing island growth at small island sizes experimentally.
- Stabilization of small islands in combination with ELMs causes flux pumping which can help one to maintain favourable q-profiles in high-performance discharges [12, 13].
- One of the problems associated with mode growth is locking of the island. Locking typically occurs at a given island width [1]. In ITER, locking is expected to start at island sizes well below the saturated island width w_{sat}. Stabilization of a mode at a certain width below the threshold island size for mode locking can be used to prevent locking of the mode.
- Having a small island present in the plasma, with a stabilized width, ensures that disturbances of the island width and unexpected mode growth due for example to other MHD modes are compensated.
- Preemptive stabilization of an island at a small island width would allow one to limit the consumed ECRH/ECCD power for mode suppression and guarantees that the stabilized mode remains in steady state. This would also have benefits for the power balance and the remaining available power for other heating and current drive tasks.
- For scenario development it could be beneficial to stabilize an island at a small size and keep it controlled at that size in a plasma with relatively low β. After the mode has been stabilized, the plasma can be maneuvered into a higher β regime.
- Hypothetically, a small magnetic island with a controlled size can also be used for interplay with the transport processes in a tokamak plasma.

In conclusion, application of the described methods in present-day tokamaks will provide important information on the dynamics of small magnetic islands, which can as well apply for ITER. The most important point, which could be investigated when enabling the stabilization of a small island is an assessment of the validity of the GRE at small island widths. Experimental identification of the dynamics of small islands sizes would by any means be desirable. Such validation could benefit of the application of advanced nonlinear system identification techniques in closed-loop experiments adopting relatively simple controllers. The extended model knowledge obtained from these experiments can in turn be used to optimize the NTM controllers further towards a design which incorporates more model knowledge such as the feedback linearizing controller.

Acknowledgments

The work in this paper has been performed within the framework of the NWO-RFBR Centre of Excellence (grant 047.018.002) on Fusion Physics and Technology. This work, supported by NWO, ITER-NL and the European Communities under the contract of the Association EURATOM/FOM, was carried out within the framework of the European Fusion Programme. The views and opinions expressed herein do not necessarily reflect those of the European Commission.

References

[1] La Haye R.J. 2006 Neoclassical tearing modes and their control *Phys. Plasmas* **13** 055501
[2] Hender T.C. *et al* 2007 Chapter 3: MHD stability, operational limits and disruptions *Nucl. Fusion* **47** S128–202
[3] Sauter O. *et al* 2002 Control of neoclassical tearing modes by sawtooth control *Phys. Rev. Lett.* **88** 105001
[4] Zohm H. *et al* 1999 Experiments on neoclassical tearing mode stabilization by ECCD in ASDEX Upgrade *Nucl. Fusion* **39** 577
[5] Prater R. 2004 Heating and current drive by electron cyclotron waves *Phys. Plasmas* **11** 2349–76
[6] Sauter O., Henderson M.A., Ramponi G., Zohm H. and Zucca C. 2010 On the requirements to control neoclassical tearing modes in burning plasmas *Plasma Phys. Control. Fusion* **52** 025002
[7] Humphreys D.A., Ferron J.R., La Haye R.J., Luce T.C., Petty C.C., Prater R. and Welander A.S. 2006 Active control for stabilization of neoclassical tearing modes *Phys. Plasmas* **13** 056113
[8] Isayama A. *et al* and the JT-60 Team 2003 Achievement of high fusion triple product, steady-state sustainment and real-time NTM stabilization in high-β_p ELMy H-mode discharges in JT-60U *Nucl. Fusion* **43** 1272–8
[9] Isayama A. *et al* and the JT-60 Team 2009 Neoclassical tearing mode control using electron cyclotron current drive and magnetic island evolution in JT-60U *Nucl. Fusion* **49** 055006
[10] Hennen B.A., Westerhof E., Nuij P.W.J.M., Oosterbeek J.W., de Baar M.R., Bongers W.A., Bürger A., Thoen D.J., Steinbuch M. and the TEXTOR team 2010 Real-time control of tearing modes using a line-of-sight electron cyclotron emission diagnostic *Plasma Phys. Control. Fusion* **52** 104006
[11] Oosterbeek J.W. *et al* 2008 A line-of-sight ECE receiver for ECRH feedback control of tearing modes *Rev. Sci. Instrum.* **79** 093503
[12] King J.D., La Haye R.J., Petty C.C., Osborne T.H., Lasnier C.J. and others 2011 Magnetic island evolution due to ELM-NTM coupling in DIII-D *Proc. 38th EPS Conf. on Plasma Physics (Strasbourg, France, 2011)* http://ocs.ciemat.es/EPS2011PAP/pdf/P2.087.pdf
[13] Petty C.C., Austin M.E., Holcomb C.T., Jayakumar R.J., La Haye R.J., Luce T.C., Makowski M.A., Politzer P.A. and Wade M.R. 2009 Magnetic-flux pumping in high-performance, stationary plasmas with tearing modes *Phys. Rev. Lett.* **102** 045005
[14] Shimada M. *et al* 2007 Progress in the ITER physics basis; Chapter 1: overview and summary *Nucl. Fusion* **47** S1–17
[15] Wilson H.R. 2008 Neoclassical tearing modes *Trans. Fusion Sci. Technol.* **53** 152–60 http://www.carolusmagnus.net/papers/2007/docs/EI5_Wilson_paper.pdf
[16] Waelbroeck F.L., Connor J.W. and Wilson H.R. 2001 Finite larmor-radius theory of magnetic island evolution *Phys. Rev. Lett.* **87** 215003
[17] De Lazzari D. and Westerhof E. 2009 On the merits of heating and current drive for tearing mode stabilization *Nucl. Fusion* **49** 075002
[18] De Lazzari D. and Westerhof E. 2010 On the merits of heating and current drive for tearing mode stabilization *Nucl. Fusion* **50** 079801 (erratum)
[19] Slotine J.J.E. and Li W. 1991 *Applied Nonlinear Control* (Englewood Cliffs, NJ: Prentice Hall)
[20] Khalil H.K. 2002 *Nonlinear Systems* 3rd edn (Upper Saddle River, NJ: Prentice Hall)
[21] Rutherford P.H. 1973 Nonlinear growth of the tearing mode *Phys. Fluids* **16** 1903–8
[22] La Haye R.J. 2008 Requirements for alignment of electron cyclotron current drive for neoclassical tearing mode stabilization in ITER *Nucl. Fusion* **48** 054004
[23] Westerhof E. *et al* 2007 Tearing mode stabilization by electron cyclotron resonance heating demonstrated in the TEXTOR tokamak and the implication for ITER *Nucl. Fusion* **47** 85–90
[24] Bertelli N., De Lazzari D. and Westerhof E. 2011 Requirements on localized current drive for the suppression of neoclassical tearing modes *Nucl. Fusion* **51** 103007
[25] Poli E., Peeters A.G. and Pereverzev G.V. 2001 TORBEAM, a beam tracing code for electron-cyclotron waves in tokamak plasmas *Comput. Phys. Commun.* **136** 90
[26] Urso L. 2009 Modelling and experiments on NTM stabilisation at ASDEX Upgrade *PhD Thesis* Ludwig-Maximilians-Universität Munich
[27] La Haye R.J., Prater R., Buttery R.J., Hayashi N., Isayama A., Maraschek M.E., Urso L. and Zohm H. 2006 Cross-machine benchmarking for ITER of neoclassical tearing mode stabilization by electron cyclotron current drive *Nucl. Fusion* **46** 451–61
[28] Skogestad S. and Postlethwaite I. 2004 *Multivariable Feedback Control* 2nd edn (Chichester, West Sussex: Wiley)